Article:
Chen, W, Kemp, DB, Newton, RJ et al. (2022) Major sulfur cycle perturbations in the Panthalassic Ocean across the Pliensbachian-Toarcian boundary and the Toarcian Oceanic Anoxic Event. Global and Planetary Change, 215. 103884. p. 103884. ISSN: 0921-8181

https://doi.org/10.1016/j.gloplacha.2022.103884

Major sulfur cycle perturbations in the Panthalassic Ocean across the Pliensbachian-Toarcian boundary and the Toarcian Oceanic Anoxic Event

Wenhan Chen [a], David B. Kemp [a*], Robert J. Newton [b], Tianchen He [b], Chunju Huang [a], Tenichi Cho [c], Kentaro Izumi [d]

[a] *State Key Laboratory of Biogeology and Environmental Geology and Hubei Key Laboratory of Critical Zone Evolution, School of Earth Sciences, China University of Geosciences, Wuhan 430074, P.R. China*

[b] *School of Earth and Environment, University of Leeds, Leeds LS2 9JT, UK*

[c] *Graduate School of Creative Science and Engineering, Waseda University, Tokyo 169-8050, Japan*

[d] *Faculty and Graduate School of Education, Chiba University, 1-33 Yayoi-cho, Inage-ku, Chiba-shi, Chiba 263-8522, Japan*

*Corresponding author: David B. Kemp (davidkemp@cug.edu.cn)

Abstract

The early Toarcian Oceanic Anoxic Event (T-OAE, ~183 Ma) was characterized by marine deoxygenation and the burial of organic-rich sediments at numerous localities worldwide. However, the extent of marine anoxia and its impact on the sulfur cycle during the T-OAE is currently poorly understood. Here, stable sulfur isotopes of reduced metal-bound sulfur ($\delta^{34}S_{pyrite}$) and pyrite sulfur concentrations (S_{PY}) have been analyzed across the Pliensbachian-Toarcian boundary (Pl-To) and the T-

OAE from the Sakahogi and Sakuraguchi-dani sections (Japan), which were deposited in the deep and shallow Panthalassic Ocean, respectively. Our data reveal marked positive $\delta^{34}S_{pyrite}$ excursions of >10‰ across both the Pl-To and the T-OAE at Sakahogi, coincident with increases in S_{PY}, and a positive excursion of >20‰ at the onset of the T-OAE at Sakuraguchi-dani. Whilst the development of deep-water anoxic/euxinic conditions could have resulted in an enhanced burial of pyrite, and also partly contributed to the positive excursion of $\delta^{34}S_{pyrite}$, variations in $\delta^{34}S_{pyrite}$ at Sakahogi were most likely controlled by elevated export production and/or preservation. On the shallow shelf generally low and highly variable S_{PY} and the positive shift in $\delta^{34}S_{pyrite}$ were likely attributable mainly to elevated sedimentation rates, with redox playing only a minor role in controlling pyrite abundance. Our discovery of a positive $\delta^{34}S_{pyrite}$ excursion across the Pl-To at Sakahogi indicates a hitherto unrecognized perturbation to the deep-water sulfur cycle, potentially associated with increased seafloor organic matter flux and pyrite burial at this time, consistent with a transient interval of anoxia.

1. Introduction

The early Toarcian Oceanic Anoxic Event (T-OAE, ~183 Ma) (Jenkyns, 1988, 2010) was an interval of marked environmental change in the Early Jurassic. The event was characterized by the widespread accumulation of

organic-rich sediments (Jenkyns, 1988), extinction (particularly for benthos) (Wignall et al., 2005; Jiang et al., 2020), an increase in seawater temperature (Bailey et al., 2003; Ruebsam et al., 2020), enhanced hydrological cycling (Izumi et al., 2018a), and increased continental weathering (Cohen, et al., 2004; Kemp et al., 2020). An abrupt negative carbon isotope excursion (NCIE) associated with the T-OAE has been recognized globally in both organic and inorganic carbon reservoirs (Hesselbo et al., 2000, 2007; Kemp et al., 2005; Izumi et al., 2012; Ikeda et al., 2018; Chen et al., 2021). This NCIE has been interpreted as a massive injection of ^{12}C-enriched carbon into the biosphere, potentially from volcanism from the Karoo-Ferrar Large Igneous Province, and possibly also via the release of thermogenic (McElwain et al., 2005; Svensen et al., 2007; Heimdal et al., 2021), and/or biogenic methane (Hesselbo et al., 2000; Kemp et al., 2005; Ruebsam et al., 2019). A similar, but smaller magnitude, NCIE has also been noted at the Pliensbachian-Toarcian boundary (Pl-To; Suan et al., 2008, 2010; Littler et al., 2010; Bodin et al., 2016), which was also associated with ecological stress and seawater warming (Harries and Little, 1999; Jiang et al., 2020; Ruebsam et al., 2020).

The carbon and sulfur cycles are intimately linked because organic carbon is essential for sulfate reduction, and there is an approximately constant ratio of organic-carbon to pyrite-sulfur burial in normal marine sediments (Berner, 1970, 1982). These coupled cycles are valuable

indicators of marine redox, which directly impact marine life (e.g. Danise et al., 2015). Carbon cycle perturbations have been reported worldwide during the T-OAE, but research on the sulfur cycle and its isotopic expression across the T-OAE is limited. Because of the negligible fractionation of $\delta^{34}S$ between carbonate-associated sulfate (CAS), i.e. sulfate bound into carbonate lattices, and dissolved seawater sulfate, S-isotopes derived from CAS ($\delta^{34}S_{CAS}$) can accurately trace perturbations to the marine sulfur cycle (Burdett et al. 1989). Previous work on the T-OAE has revealed positive shifts in $\delta^{34}S_{CAS}$ from a handful of sections in the Tethyan realm, which can be attributed to the increased burial of pyrite during expanded seawater deoxygenation under generally low seawater sulfate (SO_4^{2-}) concentrations conditions (Gill et al., 2011; Newton et al., 2011). In the well-studied Yorkshire T-OAE section (UK), for instance, a $\delta^{34}S_{CAS}$ shift of ~6‰ is recorded (Newton, et al., 2011). A similar shift (~5‰) was also recognized in Dotternhausen (Germany) in belemnites (Gill et al., 2011). Away from the Northern Europe, a positive shift of ~6‰ in $\delta^{34}S_{CAS}$ was recorded from Monte Sorgenza, Italy, deposited on the northwest margin of Tethys (Gill et al., 2011). Outside of Europe, the only data thus far presented are from Tibet (Southwest Tethyan realm), where a positive $\delta^{34}S_{CAS}$ excursion of ~19‰ is recorded (Newton et al., 2011).

Pyrite is the most abundant stable metal-sulfide preserved in marine sediments. S-isotope records measured from sedimentary pyrite ($\delta^{34}S_{pyrite}$)

offer a useful complementary method to that of $\delta^{34}S_{CAS}$ for reconstructing marine sulfur cycle dynamics and redox conditions in deep time, particularly in sections that are not carbonate dominated (Strauss, 1997). Records of $\delta^{34}S_{pyrite}$ can, however, be influenced by factors unrelated to redox and that instead provide insights into the nature of (and changes to) depositional conditions (e.g. Pasquier et al., 2021; Houghton et al., 2022). Thus far, no research has been conducted on $\delta^{34}S_{pyrite}$ and S_{PY} changes across both the Pl-To and the T-OAE.

Due to watermass restriction of basins on the Northern Europe (e.g. Dickson et al., 2017), the prolonged anoxia and/or euxinia inferred from these sites during the T-OAE from numerous lines of geochemical evidence (e.g. McArthur et al., 2008; Pearce et al., 2008) is unlikely to be representative of redox conditions in the global ocean (e.g. McArthur, 2019). Mo- and Tl-isotope data suggest an overall increase in the extent of anoxic/euxinic waters during the T-OAE (Dickson et al., 2017; Them et al., 2018). Nevertheless, the true extent of anoxia and the redox conditions of areas outside of Europe are largely unknown. In particular, the response of the Panthalassic Ocean (the largest ocean to have existed) during the T-OAE is uncertain. Moreover, despite the evidence for a marked carbon cycle perturbation across the Pl-To (e.g. Hesselbo et al., 2007; Littler et al., 2010; Ikeda et al., 2018), the coeval sulfur cycle and redox response to this event are unclear. In this study, we present the first $\delta^{34}S_{pyrite}$ and S_{PY} record

of the Panthalassic Ocean based on analysis of two sections (Sakuraguchi-dani and Sakahogi) deposited in widely differing water depths and analyze the marine sulfur cycle from the latest Pliensbachian to the early Toarcian.

2. Geological setting

Lower Jurassic siliciclastic sedimentary rocks of the Toyora Group crop out in the Toyora area of Yamaguchi Prefecture, southwest Japan (Fig. 1). The Nishinakayama Formation of the Toyora Group consists mainly of shallow marine silty mudstones and sandstones (Nakada and Matsuoka, 2011) and is well exposed at Sakuraguchi-dani (Izumi et al., 2020; Figs. 1C and 2A). The Pliensbachian to Toarcian age of this succession is well constrained by ammonite biostratigraphy (Hirano, 1973; Tanabe, 1991; Nakada and Matsuoka, 2011), and a >35m thick record of the early Toarcian negative carbon isotope ($\delta^{13}C$) excursion is also recorded, which chemostratigraphically constrains the succession (Izumi et al., 2012; Kemp and Izumi, 2014; Izumi et al., 2018a; Fig. 2A).

The upper Pliensbachian to lower Toarcian deep-sea sedimentary succession of the Inuyama area (Aichi and Gifu Prefectures) consists mainly of bedded cherts (Fig. 1D). The Sakahogi section of the Inuyama area was deposited in the deep Panthalassic Ocean, likely below carbonate compensation depth (Matsuda and Isozaki, 1991). The Sakahogi succession comprises green-grey bedded chert with two distinctive black

bedded chert and black shale intervals, both associated with CIEs (Ikeda et al., 2018; Fig. 2B). Cyclostratigraphy (Ikeda and Hori, 2014) and radiolarian biostratigraphy (Hori, 1990) indicate that the lower interval represents the Pliensbachian-Toarcian boundary and the upper interval represents the T-OAE (Ikeda et al., 2018; see also Kemp et al., 2022; Fig. 2B).

3. Analytical methods

Pyrite sulfur from 118 samples (77 from Sakuraguchi-dani and 41 from Sakahogi) was extracted using the chromium reduction method (Canfield et al., 1986). Seventy-four of these samples (35 from Sakuraguchi-dani and 39 from Sakahogi) were analyzed for $\delta^{34}S_{pyrite}$. The bulk sample powder (1-2g) was treated with ~40 mL of 1 M reduced chromium chloride ($CrCl_2$) solution and 20 mL of 6N HCl for 4 hours in a specialized pyrite extraction line at the Cohen Laboratory (University of Leeds), and the evolved hydrogen sulfide (H_2S) was purged under a nitrogen atmosphere before being trapped as Ag_2S by bubbling through an $AgNO_3$ solution (0.1M). The weight of sulfide sulfur was acquired using stoichiometric calculations on the Ag_2S mass. For isotope analysis, ~0.4 mg Ag_2S was sealed into a tin capsule with excess V_2O_5, followed by online combustion to 1050℃ under helium flow to convert to SO_2 for isotopic determination. This work was carried out at the State Key Laboratory of Biogeology and Environmental

Geology, China University of Geosciences (Wuhan), using a Thermo Delta V Plus isotope ratio mass spectrometer coupled to a Flash elemental analyzer. Sulfur isotopes are expressed in standard delta notation (δ) as per mil (‰) deviations from Vienna Canyon Diablo Troilite (VCDT). Analytical error was ~0.1‰ (1σ) based on repeated analyses of three IAEA (International Atomic Energy Agency) standard samples: IAEA-S-1 (-0.3‰), IAEA-S-2 (+22.65‰) and IAEA-S-3 (-32.5‰).

4. Results

The $\delta^{34}S_{pyrite}$ profiles at Sakahogi and Sakuraguchi-dani show broadly similar trends and features, though with distinct differences in absolute values and the magnitude of changes (Fig. 2). At Sakahogi, a marked positive $\delta^{34}S_{pyrite}$ shift with a magnitude of 11.4‰ is observed across the T-OAE (Fig. 2B), compared to a larger excursion of 24.6‰ at Sakuraguchi-dani (not including an outlying value at ~7 m; Fig. 2A). A prominent shift with a similar magnitude (12.3‰) occurs across the Pl-To at Sakahogi (Fig. 2B). The $\delta^{34}S_{pyrite}$ shifts in both sections are coeval with the respective CIEs and increased TOC. The pre- and post-excursion baseline values at Sakahogi vary between ~-50‰ and ~-42‰, in contrast to more positive baseline values (~-28‰ to ~-21‰) at Sakuraguchi-dani. In comparison to previously published $\delta^{34}S_{CAS}$ data, the excursion magnitude we observe in $\delta^{34}S_{pyrite}$ across the T-OAE (>10‰) is larger than that observed in $\delta^{34}S_{CAS}$

(~6‰) from Europe (Figs. 3C, 3D and 3E). The excursion magnitudes at Sakuraguchi-dani and Sakahogi fall either side of the magnitude calculated from Tibet by Newton et al. (2011) (~19‰; Fig. 3F). Notwithstanding marked spatial differences in $\delta^{34}S_{CAS}$ excursion magnitudes across the T-OAE, the pre-excursion values are similar (~16‰ to ~20‰) between Europe and Tibet (Fig. 3).

At Sakahogi, S_{PY} values fluctuate through the succession and vary from ~0.01 to ~8.45%, with a mean of ~0.71% (Fig. 2B). There is a slight increase across the Pl-To and a marked rise (up to ~8.45% at 224 cm) in the T-OAE interval, coincident with pronounced shifts in $\delta^{13}C_{org,}$ TOC, and $\delta^{34}S_{pyrite}$. Above this, S_{PY} drops abruptly to ~0.01% (Fig. 2B). At Sakuraguchi-dani S_{PY} values are lower and highly variable, ranging from ~0.01 to ~1.50%, with a mean of ~0.37% (Fig. 2A). Although relatively variable, a general increase to ~1.38% from the onset of the T-OAE is observable, followed by a decreasing trend up-section (Fig. 2A).

5. Discussion

Sulfide in sediments primarily forms via bacterial sulfate reduction (BSR):

$$SO_4^{2-} + 2CH_2O \rightarrow H_2S + 2\ HCO_3^- \quad (1)$$

The sulfide generated then reacts with available highly reactive Fe (Fe_{HR}) to form pyrite (Rickard 1995). Pyrite is depleted in ^{34}S relative to

sulfate, and thus a significant isotopic fractionation ($\triangle^{34}S=\delta^{34}S_{SO4}-\delta^{34}S_{pyrite}$) between the parent marine sulfate and pyrite occurs during BSR. Models of the marine sulfur cycle behavior across the Ediacaran-Cambrian and the late Hirnantian indicate that globally enhanced pyrite burial would lead to elevated $\delta^{34}S_{pyrite}$ values under low marine sulfate conditions (e.g. Fike and Grotzinger, 2008; Hammarlund et al., 2012), and such enhanced pyrite burial may have characterized the early Toarcian ocean (Newton et al., 2011). However, recent work has shown that local/regional factors can act as significant, and perhaps dominant, controls on $\delta^{34}S_{pyrite}$ in marine sediments (e.g. Fry et al., 1988; Canfield, 1991; Leavitt et al., 2013; Pasquier et al., 2017, 2021; Lang et al., 2020; Liu et al., 2021; Houghton et al., 2022). As such, the interpretation of $\delta^{34}S_{pyrite}$ records demands careful evaluation of both local and global drivers of marine sulfur cycling.

5.1 Sedimentation rates

Increased sedimentation rates can decrease the connectivity of sedimentary pore water with the overlying seawater, limiting diffusional exchange and reducing (or preventing) the resupply of seawater sulfate during BSR and pyrite formation. Higher sedimentation rates can also increase the supply of highly reactive iron to the sediment relative to organic matter and sulfate, ensuring more efficient trapping of dissolved hydrogen sulfide as solid iron sulfides (Liu et al., 2021). Both these effects

result in increases in $\delta^{34}S_{pyrite}$ via more closed system behavior at higher sedimentation rates (Canfield, 1991; Pasquier et al., 2017, 2021; Liu et al., 2019; Liu et al., 2021; Houghton et al., 2022).

Because of the different water depths and relative distance from land, the two study sites experienced very different rates of sedimentation prior to the Toarcian NCIE, with higher sedimentation rates at Sakuraguchi-dani than at Sakahogi. This is consistent with more negative pre-excursion baseline values of $\delta^{34}S_{pyrite}$ at the deep water Sakahogi site (around -50‰; Fig. 2B), when compared to those at Sakuraguchi-dani on the shallow and more rapidly accumulating shelf (around -28‰; Fig. 2A).

The globally synchronous Toarcian NCIE allows direct comparison of sedimentation rates between Sakahogi and Sakuraguchi-dani during the event. At the shallower Sakuraguchi-dani site the NCIE is ~35 m thick, and it is just ~0.75 m thick at Sakahogi. The Toarcian event has been linked to increases in the hydrological cycle, weathering and terrigenous sediment supply (e.g., Cohen et al., 2004; Izumi et al., 2018a; Kemp et al., 2020), and sedimentation rates are likely to have increased at Sakuraguchi-dani during this period of environmental perturbation (see for example Izumi et al., 2018a; Kemp et al., 2019). A marked increase in sedimentation rate during the early Toarcian event is therefore the likely explanation for the larger positive excursion in $\delta^{34}S_{pyrite}$ at Sakuraguchi-dani. Evidence for a marked increase in sedimentation rate within the T-OAE at Sakuraguchi-

dani occurs in the form of a lithological change from mudstone to silty mudstones with sandstone (Fig. 2A; Izumi et al., 2018a), and a coeval increase in phytoclasts (indicative of increased terrestrial delivery from rivers; see Kemp et al., 2019). Indeed, the positive excursion in $\delta^{34}S_{pyrite}$ closely corresponds with the increase in sandstone and phytoclast content at Sakuraguchi-dani, providing further evidence of a sedimentation rate control (Figs. 2A and S1). Additionally, although fluctuations of shallow-water redox conditions may have contributed to the high variability in S_{PY} at Sakuraguchi-dani (see Section 5.5 below), the overall low S_{PY} recorded in this section could have largely been a consequence of high sedimentation rates. In this case, and as noted above, porewater sulfate is more rapidly depleted due to the suppression of sulfate supply from the overlying water column (e.g. Lang et al., 2020).

$\delta^{34}S_{pyrite}$ at Sakahogi was maintained at much more negative values both prior to and during the early Toarcian event because sedimentation rates were significantly lower than those on the shelf. These low sedimentation rates in an open and quiescent environment, combined with the development of anoxic waters (Kemp et al., 2022), would have favored the open system supply of sulfate for BSR and large isotopic fractionations from seawater similar to the low $\delta^{34}S_{pyrite}$ values from modern euxinic settings like the Black Sea (Wijsman et al., 2001b; Johnston et al., 2008).

The overall comparisons between the sites are consistent with

measurements of $\delta^{34}S_{pyrite}$ at sites with contrasting water depths off the New Zealand coast (Pasquier et al., 2021), and with $\delta^{34}S_{pyrite}$ measurements across cycles of glacial and interglacial sedimentation in the Mediterranean (Pasquier et al., 2017). Our findings are also consistent with results from a Pleistocene shallow-water section from Italy, which emphasizes the role of sedimentation rates associated with glacial-interglacial eustatic sea-level changes, regional climate and local tectonics in controlling sedimentary $\delta^{34}S_{pyrite}$ (Houghton et al., 2022).

5.2 Organic matter supply

Culture experiments have shown that cell-specific sulfate reduction rates (csSRR) can influence sulfur-isotope fractionation, whereby faster rates of csSRR correspond to decreased isotopic fractionation (Sim et al., 2011; Leavitt, et al., 2013). This mechanism may have come into play at Sakahogi, where sedimentation rates likely remained low throughout the studied interval. An increased delivery rate of organic matter to the seafloor could elevate csSRR rates, thus reducing isotopic fractionation and elevating $\delta^{34}S_{pyrite}$ values (e.g. Pasquier et al., 2021). In addition, the source of organic matter (marine versus terrestrial) likely plays a key role in influencing the sulfate reduction rate, because marine biomass is more bioavailable for microorganisms within marine sediments compared to more refractory terrestrial organic matter (Toth and Lerman, 1977;

Mollenhauer and Eglinton, 2007). Given the strong correlations between TOC and $\delta^{34}S_{pyrite}$ at Sakahogi (Fig. 4B), it is likely that accelerated csSRR linked to an increased supply of more bioavailable organic carbon played an important role in generating the positive excursions in $\delta^{34}S_{pyrite}$ at Sakahogi at both the Pl-To boundary (TOC vs $\delta^{34}S_{pyrite}$ $R^2 = 0.79$) and the early Toarcian NCIE (TOC vs $\delta^{34}S_{pyrite}$ $R^2 = 0.55$).

At Sakuraguchi-dani, there is no correlation between TOC and $\delta^{34}S_{pyrite}$ (R^2=0.09; Fig. 4A), indicating that organic matter supply had negligible control on the positive excursion in $\delta^{34}S_{pyrite}$ across the T-OAE. This is consistent with a greater delivery of more refractory terrestrial organic matter in this shallow nearshore setting during the T-OAE (Kemp and Izumi, 2014; Izumi et al., 2018a; Kemp et al., 2019).

5.3 Marine sulfate concentrations [SO_4^{2-}] and isotopic composition ($\delta^{34}S_{SO4}$)

Isotopic fractionation ($\triangle^{34}S$) during microbial sulfate reduction is up to 70‰ in modern marine sediments through a series of intermediate reduction steps when marine sulfate replenishment is sufficient (Canfield and Raiswell, 1999). However, empirical work from 81 modern aqueous systems indicates that such isotopic fractionation would decrease significantly when seawater [SO_4^{2-}] is below 5 mM (Algeo et al., 2015). Experimental data from microbial cultures suggest that the isotopic

fractionation will decrease proportionally with the concentration of seawater sulfate when [SO_4^{2-}] is <2 mM, and will be <10‰ when [SO_4^{2-}] is <0.2 mM (Canfield, 2001; Habicht et al., 2002, 2005). Thus, a small oceanic sulfate reservoir could be an important driver for decreases in isotopic fractionation ($\triangle^{34}S$) and elevated $\delta^{34}S_{pyrite}$.

Modelling of the Toarcian $\delta^{34}S_{CAS}$ record indicates that seawater [SO_4^{2-}] may have been 0.6–8 mM at this time (Gill et al., 2011; Newton et al., 2011; Han et al., 2022), suggesting that this has the potential to be a driver for changes in $\delta^{34}S_{pyrite}$. The maximum $\delta^{34}S_{pyrite}$ at Sakahogi is around -35‰. When compared to the minimum possible contemporaneous CAS value of +24‰ (Newton et al., 2011) this means that there is a minimum isotopic fractionation ($\triangle^{34}S$) of 59‰, which is inconsistent with sulfate limitation being the main driver of change in $\delta^{34}S_{pyrite}$. Thus, the different $\delta^{34}S_{pyrite}$ excursion magnitudes between Sakahogi and Sakuraguchi-dani suggest that the effect of a smaller sulfate reservoir was limited, perhaps only being discernable in the small drift to more positive values in the $\delta^{34}S_{pyrite}$ baseline for both sections.

During the T-OAE, CAS isotope records show that there was a large change to more positive $\delta^{34}S_{SO4}$ of between approximately 6 and 20‰, depending on the location (Gill et al., 2011; Newton et al., 2011; Fig. 3). This ostensibly has the potential to influence the $\delta^{34}S_{pyrite}$ record. However, two features of our $\delta^{34}S_{pyrite}$ data suggest that this had little or no influence:

335 Firstly, elevated $\delta^{34}S_{SO4}$ continued until the end of the Toarcian after the
336 NCIE, whereas the positive $\delta^{34}S_{pyrite}$ excursions we observe ended within
337 the NCIE (Fig. 3). Secondly, there is no apparent excursion in $\delta^{34}S_{CAS}$
338 across the Pliensbachian-Toarcian boundary event (Gill et al., 2011; Han et
339 al., 2022). Hence, these two parameters seem divorced for this time interval.
340
341 5.4 Temperature
342 Increased seawater temperature associated with the emission of large
343 amounts of CO_2 to the ocean-atmosphere system (e.g. Bailey et al., 2003;
344 Suan et al., 2008; Ruebsam et al., 2020) could have influenced $\delta^{34}S_{pyrite}$ –
345 for example by affecting rates of microbial sulfate reduction. However, it
346 is difficult to predict *a priori* how temperature could have affected
347 fractionation and the isotopic composition of pyrite because different
348 sulfate-reducing populations tend to show widely differing responses to
349 change in seawater temperature, with differing fractionation effects, also
350 linked to organic matter type/quality (e.g. Canfield et al., 2006; Westrich
351 and Berner, 1988). Evaluating the impact of temperature on $\delta^{34}S_{pyrite}$ in
352 these records would require detailed investigation and may not be possible
353 given the uncertainties. We suggest, however, that temperature changes are
354 likely to be insignificant relative to the controls exerted by sedimentation
355 rate and organic matter supply.
356
357 5.5 Anoxia

Distinct enrichments of redox-sensitive trace elements such as Mo and U at Sakahogi, coupled with markedly elevated TOC/P ratios, indicate the presence of euxinic conditions across the Pl-To and T-OAE at Sakahogi (Kemp et al., 2022). This is further supported by framboid size distribution data and pyrite analysis based on Mössbauer spectroscopy from the nearby Katsuyama section (Wignall et al., 2010; Sato et al., 2012; Fig. 1D). All these datasets suggest intensified anoxia developed close to the Pl-To boundary and extended through the Toarcian event (e.g., Kemp et al., 2022). At Sakuraguchi-dani, there is only limited evidence for ephemeral anoxia across the T-OAE from laminated sediments, trace elements and framboid data, and the environment likely remained predominantly oxic (Izumi et al., 2012, 2018b; Kemp and Izumi, 2014).

Pyrite formation and burial depends on supplies of sulfate, organic matter and highly reactive iron (Berner, 1982; Morse and Berner, 1995). Increased Fe_{HR} supply is likely to have played a part in elevating S_{PY} in the deep-water Sakahogi section facilitated by an anoxic reactive iron shuttle. This mechanism transports reactive iron from basin margin sediments and concentrates it in deeper waters (Wijsman et al., 2001a; Anderson and Raiswell, 2004; Lyons and Severmann, 2006). Hydrothermal activity can also deliver Fe_{HR} to support pyrite formation in the deep ocean (Poulton and Canfield, 2011). However, deposition of the bedded cherts at Inuyama was likely well away from the influence of any hydrothermal venting

(Matsuda and Isozaki, 1991), and the preservation of primary and globally representative isotopic signals such as Os-isotopes at Inuyama (e.g. Kuroda et al., 2010) further suggests limited influence of hydrothermal fluids.

The high S_{PY} and markedly elevated TOC across the T-OAE at Sakahogi (up to 8.45% and 34.2%, respectively) suggests increased organic carbon supply and/or preservation on the seafloor. This could have fueled BSR under anoxic conditions in the deep waters (Fig. S2). Paleomagnetic data suggest a low latitude depositional setting during the Toarcian event, close to the equatorial divergence zone (Shibuya and Samejima, 1986; Fujii et al., 1993; Ando et al., 2001; Fig. 1A). Here, high surface ocean productivity could have been maintained via optimum water temperatures and nutrient supply from upwelling. Cyclostratigrahic analysis of chert bed thicknesses in Inuyama across the T-OAE also suggests enhanced surface ocean primary productivity associated with orbitally controlled variations in summer monsoon intensity and nutrient supply to Panthalassa (Ikeda and Hori, 2014). Equally, previous work has speculated that TOC enrichment in the Inuyama area could have been further facilitated by a shorter export pathway owing to deposition on the mesopelagic to upper bathyal seafloor of a volcanic seamount rather than on the abyssal seafloor (Gröcke et al., 2011), though direct evidence for this is lacking. More recent analysis based on Cd/Mo and Co*Mn variations (indicative of the mechanisms of organic enrichment; see

Sweere et al., 2016 for details) at Sakahogi across the T-OAE suggests that anoxia enhanced the preservation of deep-water organic carbon at this site, so this may have been more important than productivity as a control on the high TOC content in these black cherts (Kemp et al., 2022).

At Sakuraguchi-dani, a paucity of suitable data precludes detailed insight into primary productivity variations, so the degree to which this might control sulfur cycling in this section are unclear. Nevertheless, the combined effects of high sedimentation rates, lower concentration of mainly terrestrial (i.e., refractory) organic carbon, and the generally suboxic-oxic depositional conditions (Kemp and Izumi, 2014; Kemp et al., 2019) can explain the much lower overall S_{PY} at this site. The high variability in S_{PY} during the T-OAE interval at Sakuraguchi-dani is consistent with ephemeral anoxia/euxinia inferred from the available relatively low-resolution ichnofabric index and framboidal pyrite size distribution data (Izumi et al., 2012; Izumi et al., 2018b).

In modern anoxic systems $\delta^{34}S_{pyrite}$ can be more negative than pyrite deposited in other settings, creating larger isotope fractionations ($\Delta^{34}S$ of ~60‰) than the long-term average record for the Jurassic of ~40‰ (e.g. Lyons, 1997; c.f. Wu et al., 2010). At both Sakuraguchi-dani and Sakahogi the shift during the NCIE is to more positive values suggesting that other controls were more dominant. This observation is important for efforts to model sulfur cycle behavior during anoxic events where larger isotopic

fractionations ($\Delta^{34}S$) between sulfate and sulfide are used based on values from modern basins (e.g. Owens et al., 2013). The relationships between anoxia and $\delta^{34}S_{pyrite}$ seen at Sakuraguchi-dani and Sakahogi suggest that $\Delta^{34}S$ may stay the same or decrease because of the overriding effects of increased sedimentation rates and enhanced organic matter supply during warming driven anoxic events. This should be taken into account in future modelling efforts.

Conclusions

Our work presents the first pyrite sulfur isotope data across the Pl-To and T-OAE. The direct comparison of data from the same ocean but at widely differing water depths helps to emphasize the complexity and sensitivity of sedimentary environmental controls on $\delta^{34}S_{pyrite}$, and the utility of this proxy for understanding environmental change over Earth history.

Marked positive shifts in Panthalassic $\delta^{34}S_{pyrite}$ across the T-OAE were likely predominantly controlled by increased sedimentation rates on the shallow shelf of the Sakuraguchi-dani section, and by elevated organic carbon flux to the seafloor in the deep ocean Sakahogi section (possibly augmented by deep ocean anoxia). This response probably maintained or decreased the isotopic fractionation between seawater and buried pyrite contrary to the conditions imposed in many sulfur cycling modelling

studies, and likely stemmed from the overriding effects of an increased hydrological cycle and increased productivity during these warming driven oceanic anoxic events.

The high sedimentation rates, increased proportion of refractory terrestrial carbon and generally more oxygenated setting at Sakuraguchi-dani resulted in low pyrite concentrations overall and only muted enhancement during the T-OAE interval. At Sakahogi, pyrite concentrations were massively elevated during the T-OAE from low background values due to a combination of enhanced ocean surface productivity and/or favorable preservation conditions for organic carbon, and a lack of dilution from siliciclastic material. This represents a big increase in the pyrite flux of sulfur to deep waters at this site during the T-OAE.

Our data are the first to demonstrate a $\delta^{34}S$ perturbation across the Pl-To boundary present in the deep water Sakahogi section, which points to a period of elevated seafloor organic matter flux and high pyrite burial at this time, coincident with a transient interval of anoxia. Overall, our work emphasizes that $\delta^{34}S_{pyrite}$ responds mostly to regional rather than global drivers in shallow and deep settings.

Acknowledgements

We are grateful to Yijun Xiong for the pyrite extraction at the Cohen

Laboratory, University of Leeds. We thank Zihu Zhang for $\delta^{34}S_{pyrite}$ analyses at the State Key Laboratory of Biogeology and Environmental Geology, China University of Geosciences (Wuhan). This work was supported by the National Natural Science Foundation of China (Grant No. 41888101 and No. 41772029), and the National Recruitment Program for Young Professionals (P.R. China) to DBK. RJN and TH were supported by grant NE/N018559/1 from the Natural Environment Research Council. This manuscript is a contribution to the Integrated Understanding of the Early Jurassic Earth System and Timescale (JET) ICDP project and IGCP 739.

Appendix A. Supplementary material

Supplementary material related to this article can be found on-line at https://

References

Algeo, T.J., Luo, G., Song, H., Lyons, T.W., Canfield, D.E., 2015. Reconstruction of secular variation in seawater sulfate concentrations. Biogeosciences 12, 2131–2151.

Anderson, T.F., Raiswell, R., 2004. Sources and mechanisms for the enrichment of highly reactive iron in euxinic Black Sea sediments. Am. J. Sci. 304, 203–233.

Ando, A., Kodama, K., Kojima, S., 2001. Low-latitude and Southern

491 Hemisphere origin of Anisian (Triassic) bedded chert in the Inuyama
492 area, Mino terrene, Central Japan. J. Geophys. Res. 106, 1973–1986.
493 Bailey, T.R., Rosenthal, Y., McArthur, J.M., van de Schootbrugge, B.,
494 Thirlwall, M.F., 2003. Paleoceanographic changes of the Late
495 Pliensbachian–Early Toarcian interval: a possible link to the genesis
496 of an Oceanic Anoxic Event. Earth Planet. Sci. Lett. 212 (3–4), 307–
497 320.
498 Berner, R.A., 1970. Sedimentary pyrite formation. Am. J. Sci. 268, 1–23.
499 Berner, R.A., 1982. Burial of organic carbon and pyrite sulfur in the
500 modern ocean: its geochemical and environmental significance. Am.
501 J. Sci. 282 (4), 451–473.
502 Bodin, S., Krencker, F.N., Kothe, T., Hoffmann, R., Mattioli, E.,
503 Heimhofer, U., Kabiri, L., 2016. Perturbation of the carbon cycle
504 during the late Pliensbachian–early Toarcian: New insight from high-
505 resolution carbon isotope records in Morocco. J. Afr. Earth Sci. 116,
506 89–104.
507 Burdett, J.W., Arthur, M.A., Richardson, M., 1989. A Neogene seawater
508 sulfate isotope age curve from calcareous pelagic microfossils. Earth
509 Planet. Sci. Lett. 94, 189–198.
510 Canfield, D.E., Raiswell, R., Westrich, J.T., Reaves, C.M., Berner, R.A.,
511 1986. The use of chromium reduction in the analysis of reduced
512 inorganic sulfur in sediments and shales. Chem. Geol. 54, 149–155.

513 Canfield, D.E., 1991. Sulfate reduction in deep-sea sediments. Am. J. Sci.
514 291, 177–188.
515 Canfield, D.E., Raiswell, R., 1999. The evolution of the sulfur cycle. Am.
516 J. Sci. 299, 697–723.
517 Canfield, D.E., 2001. Biogeochemistry of sulfur isotopes. Rev. Mineral.
518 Geochem. 43, 607–636.
519 Canfield, D.E., Olesen, C.A., Cox, R.P., 2006. Temperature and its control
520 of isotope fractionation by a sulfate-reducing bacterium. Geochim.
521 Cosmochim. Acta 70, 548–561.
522 Chen, W., Kemp, D.B., He, T., Huang, C., Jin, S., Xiong, Y., Newton, R.J.,
523 2021. First record of the early Toarcian oceanic anoxic event in the
524 Hebrides Basin (UK) and implications for redox and weathering
525 changes. Glob. Planet. Chang. 207, 103685.
526 Cohen, A.S., Coe, A.L., Harding, S.M., Schwark, L., 2004. Osmium
527 isotope evidence for the regulation of atmospheric CO_2 by continental
528 weathering. Geology 32 (2), 157–160.
529 Danise, S., Twitchett, R.J., Little, C.T.S., 2015. Environmental controls on
530 Jurassic marine ecosystems during global warming. Geology 43 (3),
531 263–266.
532 Dickson, A.J., Gill, B.C., Ruhl, M., Jenkyns, H.C., Porcelli, D., Idiz, E.,
533 Lyons, T.W., van den Boorn, S.H., 2017. Molybdenum-isotope
534 chemostratigraphy and paleoceanography of the Toarcian Oceanic

Anoxic Event (Early Jurassic). Paleoceanography 32 (8), 813–829.

Fike, D.A., Grotzinger, J.P., 2008. A paired sulfate–pyrite δ34S approach to understanding the evolution of the Ediacaran–Cambrian sulfur cycle. Geochim. Cosmochim. Acta 72, 2636–2648.

Fry, B., Ruf, W., Gest, H., Hayes, J.M., 1988. Sulfur isotope effects associated with oxidation of sulfide by O_2 in aqueous solution. Chem. Geol. 73, 205–210.

Fujii, J., Hattori, I., Nakajima, T., 1993. A study of radiolarian biostratigraphy and magnetostratigraphy of early Mesozoic red bedded chert, central Japan. News of Osaka Micropaleontologists 9, 71–89.

Gill, B.C., Lyons, T.W., Jenkyns, H.C., 2011. A global perturbation to the sulfur cycle during the Toarcian Oceanic Anoxic Event. Earth Planet. Sci. Lett. 321 (3–4), 484–496.

Golonka, J., 2007. Late Triassic and Early Jurassic palaeogeography of the world. Palaeogeogr. Palaeoclimatol. Palaeoecol. 244, 297–307.

Gröcke, D.R., Hori, R.S., Trabucho-Alexandre, J., Kemp, D.B., Schwark, L., 2011. An open ocean record of the Toarcian oceanic anoxic event. Solid Earth 2, 245–257.

Habicht, K.S., Gade, M., Thamdrup, B., Berg, P., Canfield, D.E., 2002. Calibration of sulfate levels in the Archean Ocean. Science 298, 2372–2374.

557 Habicht, K.S., Salling, L., Thamdrup, B., Canfield, D.E., 2005. Effect of
558 low sulfate concentrations on lactate oxidation and isotope
559 fractionation during sulfate reduction by *Archaeoglobus fulgidus*
560 strain Z. Applied and Environmental Microbiology 71, 3770–3777.
561 Hammarlund, E.U., Dahl, T.W., Harper, D.A.T., Bond, D.P.G., Nielsen,
562 A.T., Bjerrum, C.J., Schovsbo, N.H., Schönlaub, H.P., Zalasiewicz,
563 J.A., Canfield, D.E., 2012. A sulfidic driver for the end-Ordovician
564 mass extinction. Earth Planet. Sci. Lett. 331–332, 128–139.
565 Han, Z., Hu, X., He, T., Newton, R.J., Jenkyns, H.C., Jamieson, R.A.,
566 Franceschi, M., 2022. Early Jurassic long-term oceanic sulfur-cycle
567 perturbations in the Tibetan Himalaya. Earth Planet. Sci. Lett. 578,
568 117261.
569 Harries, P.J., Little, C.T.S., 1999. The early Toarcian (Early Jurassic) and
570 the Cenomanian-Turonian (Late Cretaceous) mass extinctions:
571 similarities and contrasts. Palaeogeogr. Palaeoclimatol. Palaeoecol.
572 154, 39–66.
573 Heimdal, T.H., Goddéris, Y., Jones, M.T., Svensen, H.H., 2021. Assessing
574 the importance of thermogenic degassing from the Karoo Large
575 Igneous Province (LIP) in driving Toarcian carbon cycle perturbations.
576 Nat. Commun. 12, 6221.
577 Hesselbo, S.P., Gröcke, D.R., Jenkyns, H.C., Bjerrum, C.J., Farrimond, P.,
578 Bell, H.S.M., Green, O.R., 2000. Massive dissociation of gas hydrate

579 during a Jurassic oceanic anoxic event. Nature 406 (6794), 392–395.
580 Hesselbo, S.P., Jenkyns, H.C., Duarte, L.V., Oliveira, L.C., 2007. Carbon-
581 isotope record of the Early Jurassic (Toarcian) Oceanic Anoxic Event
582 from fossil wood and marine carbonate (Lusitanian Basin, Portugal).
583 Earth Planet. Sci. Lett. 253 (3–4), 455–470.
584 Hirano, H., 1973. Biostratigraphic study of the Jurassic Toyora Group, part
585 3. Trans. Proc. Palaeont. Soc. Japan, N.S. 90, 45–71.
586 Hori, S.R., 1990. Lower Jurassic radiolarian zones of SW Japan. Trans.
587 Proc. Palaeont. Soc. Japan, N.S. 159, 562–586.
588 Houghton, J., Scarponi, D., Capraro, L., Fike, D.A., 2022. Impact of
589 sedimentation, climate and sea level on marine sedimentary pyrite
590 sulfur isotopes: Insights from the Valle di Manche section (Lower–
591 Middle Pleistocene, southern Italy). Palaeogeogr. Palaeoclimatol.
592 Palaeoecol. 585, 110730.
593 Ikeda, M., Hori, R.S., 2014. Effects of Karoo–Ferrar volcanism and
594 astronomical cycles on the Toarcian Oceanic Anoxic Events (early
595 Jurassic). Palaeogeogr. Palaeoclimatol. Palaeoecol. 410, 134–142.
596 Ikeda, M., Hori, R.S., Ikehara, M., Miyashita, R., Chino, M., Yamada, K.,
597 2018. Carbon cycle dynamics linked with Karoo-Ferrar volcanism
598 and astronomical cycles during Pliensbachian-Toarcian (Early
599 Jurassic). Glob. Planet. Chang. 170, 163–171.
600 Izumi, K., Miyaji, T., Tanabe, K., 2012. Early Toarcian (Early Jurassic)

601 oceanic anoxic event recorded in the shelf deposits in the
602 northwestern Panthalassa: evidence from the Nishinakayama
603 Formation in the Toyora area, west Japan. Palaeogeogr.
604 Palaeoclimatol. Palaeoecol. 315, 100–108.
605 Izumi, K., Kemp, D.B., Itamiya, S., Inui, M., 2018a. Sedimentary evidence
606 for enhanced hydrological cycling in response to rapid carbon release
607 during the early Toarcian oceanic anoxic event. Earth Planet. Sci. Lett.
608 481, 162–170.
609 Izumi, K., Endo, K., Kemp, D.B., Inui, M., 2018b. Oceanic redox
610 conditions through the late Pliensbachian to early Toarcian on the
611 northwestern Panthalassa margin: Insights from pyrite and
612 geochemical data. Palaeogeogr. Palaeoclimatol. Palaeoecol. 493, 1–
613 10.
614 Izumi, K., Suzuki, K., Kemp, D.B., Lizuka, T., 2020. Paleogeographic and
615 tectonic setting of the Lower Jurassic (Pliensbachian-Toarcian)
616 Nishinakayama Formation, Toyora Group, SW Japan. Geological
617 Journal 55, 862–874.
618 Jenkyns, H.C., 1988. The early Toarcian (Jurassic) anoxic event-
619 stratigraphic, sedimentary, and geochemical evidence. Am. J. Sci. 288
620 (2), 101–151.
621 Jenkyns, H.C., 2010. Geochemistry of oceanic anoxic events. Geochem.
622 Geophys. Geosyst. 11, Q03004.

623 Jiang, S., Song, H., Kemp, D.B., Dai, X., Liu, X., 2020. Two pulses of
624 extinction of larger benthic foraminifera during the Pliensbachian-
625 Toarcian and early Toarcian environmental crises. Palaeogeogr.
626 Palaeoclimatol. Palaeoecol. 560, 109998.
627 Johnston, D.T., Farquhar, J., Habicht, K.S., Canfield, D.E., 2008. Sulphur
628 isotopes and the search for life: strategies for identifying sulphur
629 metabolisms in the rock record and beyond. Geobiology 6, 425–435.
630 Kemp, D.B., Coe, A.L., Cohen, A.S., Schwark, L., 2005. Astronomical
631 pacing of methane release in the Early Jurassic period. Nature 437
632 (7057), 396–399.
633 Kemp, D.B., Izumi, K., 2014. Multiproxy geochemical analysis of a
634 Panthalassic margin record of the early Toarcian oceanic anoxic event
635 (Toyora area, Japan). Palaeogeogr. Palaeoclimatol. Palaeoecol. 414,
636 332–341.
637 Kemp, D.B., Baranyi, V., Izumi, K., Burgess, R.D., 2019. Organic matter
638 variations and links to climate across the early Toarcian oceanic
639 anoxic event (T-OAE) in Toyora area, southwest Japan. Palaeogeogr.
640 Palaeoclimatol. Palaeoecol. 530, 90–102.
641 Kemp, D.B., Selby, D., Izumi, K., 2020. Direct coupling between carbon
642 release and weathering during the Toarcian oceanic anoxic event.
643 Geology 48, 976–980.
644 Kemp, D.B., Chen, W., Cho, T., Algeo, T.J., Shen, J., Ikeda, M., 2022.

645 Deep-ocean anoxia across the Pliensbachian-Toarcian boundary and
646 the Toarcian Oceanic Anoxic Event in the Panthalassic Ocean. Glob.
647 Planet. Chang. 212, 103782.
648 Kuroda, J., Hori, R.S., Suzuki, K., Gröcke, D.R., Ohkouchi, N., 2010.
649 Marine osmium isotope record across the Triassic-Jurassic boundary
650 from a Pacific pelagic site. Geology 38, 1095–1098.
651 Lang, X., Tang, W., Ma, H., Shen, B., 2020. Local environmental variation
652 obscures the interpretation of pyrite sulfur isotope records. Earth
653 Planet. Sci. Lett. 533, 116056.
654 Leavitt, W.D., Halevy, I., Bradley, A.S., Johnston, D.T., 2013. Influence
655 of sulfate reduction rates on the Phanerozoic sulfur isotope record.
656 Proc. Natl. Acad. Sci. USA 110, 11244–11249.
657 Littler, K., Hesselbo, S.P., Jenkyns, H.C., 2010. A carbon-isotope
658 perturbation at the Pliensbachian–Toarcian boundary: evidence from
659 the Lias Group, NE England. Geol. Mag. 147 (2), 181–192.
660 Liu, X., Fike, D.A., Li, A., Dong, J., Xu, F., Zhuang, G., Rendle-Bühring,
661 R., Wan, S., 2019. Pyrite sulfur isotopes constrained by sedimentation
662 rates: Evidence from sediments on the East China Sea inner shelf
663 since the late Pleistocene. Chem. Geol. 505, 66–75.
664 Liu, J., Antler, G., Pellerin, A., Izon, G., Dohrmann, I., Findlay, A.J., Røy,
665 H., Ono, S., Turchyn, A.V., Kasten, S., Jørgensen, B.B., 2021.
666 Isotopically “heavy” pyrite in marine sediments due to high

667 sedimentation rates and non-steady-state deposition. Geology 49 (7),
668 816–821.
669 Lyons, T.W., 1997. Sulfur isotopic trends and pathways of iron sulfide
670 formation in upper Holocene sediments of the anoxic Black Sea.
671 Geochim. Cosmochim. Acta 61, 3367–3382.
672 Lyons, T.W., Severmann, S., 2006. A critical look at iron paleoredox
673 proxies: New insights from modern euxinic marine basins. Geochim.
674 Cosmochim. Acta 70, 5698–5722.
675 Matsuda, T., Isozaki, Y., 1991. Well-documented travel history of
676 Mesozoic pelagic chert in Japan: From remote ocean to subduction
677 zone. Tectonics 10, 475–499.
678 McArthur, J.M., Algeo, T.J., van de Schootbrugge, B., Li, Q., Howarth,
679 R.J., 2008. Basinal restriction, black shales, Re-Os dating, and the
680 Early Toarcian (Jurassic) oceanic anoxic event. Paleoceanography 23
681 (4), PA4217.
682 McArthur, J.M., 2019. Early Toarcian black shales: A response to an
683 oceanic anoxic event or anoxia in marginal basins? Chem. Geol. 522,
684 71–83.
685 McElwain, J.C., Wade-Murphy, J., Hesselbo, S.P., 2005. Changes in
686 carbon dioxide during an oceanic anoxic event linked to intrusion into
687 Gondwana coals. Nature 435 (7041), 479–482.
688 Mollenhauer, G., Eglinton, T.I., 2007. Diagenetic and sedimentological

689 controls on the composition of organic matter preserved in California
690 Borderland Basin sediments. Limnol. Oceanogr. 52 (2), 558–576.
691 Morse, J.W., Berner, R.A., 1995. What determines sedimentary C/S ratios?
692 Geochim. Cosmochim. Acta 59, 1073–1077.
693 Nakada, K., Matsuoka, A., 2011. International correlation of the
694 Pliensbachian/Toarcian (Lower Jurassic) ammonoid biostratigraphy
695 of the Nishinakayama Formation in the Toyora Group, southwest
696 Japan. Newsletters on Stratigraphy 44, 89–111.
697 Newton, R.J., Reeves, E.P., Kafousia, N., Wignall, P.B., Bottrell, S.H., Sha,
698 J.-G., 2011. Low marine sulfate concentrations and the isolation of
699 the European epicontinental sea during the Early Jurassic. Geology
700 39, 7–10.
701 Owens, J.D., Gill, B.C., Jenkyns, H.C., Bates, S.M., Severmann, S.,
702 Kuypers, M.M.M., Woodfine, R.G., Lyons, T.W., 2013. Sulfur
703 isotopes track the global extent and dynamics of euxinia during
704 Cretaceous Oceanic Anoxic Event 2. Proceedings of the National
705 Academy of Sciences 110, 18407–18412.
706 Pasquier, V., Sansjofre, P., Rabineau, M., Revillon, S., Houghton, J., Fike,
707 D.A., 2017. Pyrite sulfur isotopes reveal glacial−interglacial
708 environmental changes. Proc. Natl. Acad. Sci. USA 114 (23), 5941–
709 5945.
710 Pasquier, V., Bryant, R.N., Fike, D.A., Halevy, I., 2021. Strong local, not

711 global, controls on marine pyrite sulfur isotopes. Sci. Adv. 7,
712 eabb7403.
713 Pearce, C.R., Cohen, A.S., Coe, A.L., Burton, K.W., 2008. Molybdenum
714 isotope evidence for global ocean anoxia coupled with perturbations
715 to the carbon cycle during the early Jurassic. Geology 36 (3), 231–
716 234.
717 Poulton, S.W., Canfield, D.E., 2011. Ferruginous conditions: a dominant
718 feature of the ocean through Earth's history. Elements 7, 107–112.
719 Rickard D., 1995. Kinetics of FeS precipitation. Part 1: Competing reaction
720 mechanisms. Geochim. Cosmochim. Acta 59, 4367–4379.
721 Ruebsam, W., Mayer, B., Schwark, L., 2019. Cryosphere carbon dynamics
722 control early Toarcian global warming and sea level evolution. Glob.
723 Planet. Chang. 172, 440–453.
724 Ruebsam, W., Reolid, M., Sabatino, N., Masetti, D., Schwark, L., 2020.
725 Molecular paleothermometry of the early Toarcian climate
726 perturbation. Glob. Planet. Chang. 195, 103351.
727 Sato, T., Isozaki, Y., Shozugawa, K., Matsuo, M., 2012. ^{57}Fe Mössbauer
728 analysis of the Upper Triassic-Lower Jurassic deep-sea chert: Paleo-
729 redox history across the Triassic–Jurassic boundary and the Toarcian
730 oceanic anoxic event. Hyperfine Interactions 208, 95–98.
731 Scotese, C.R., 2001. Atlas of Earth History. Paleogeography, 1.
732 PALEOMAP Project, Arlington, Tex, ISBN 0-9700020-0-9, p. 52.

733 Shibuya, H., Sasajima, S., 1986. Paleomagnetism of red cherts: a case
734 study in the Inuyama area, Central Japan. J. Geophys. Res. 91, 105–
735 116.
736 Sim, M.S., Bosak, T., Ono, S., 2011. Large sulfur isotope fractionation
737 does not require disproportionation. Science 333, 74–77.
738 Strauss, H., 1997. The isotopic composition of sedimentary sulfur through
739 time. Palaeogeogr. Palaeoclimatol. Palaeoecol. 132, 97–118.
740 Suan, G., Mattioli, E., Pittet, B., Mailliot, S., Lécuyer, C., 2008. Evidence
741 for major environmental perturbation prior to and during the Toarcian
742 (Early Jurassic) oceanic anoxic event from the Lusitanian Basin,
743 Portugal. Paleoceanography 23 (1), PA1202.
744 Suan, G., Mattioli, E., Pittet, B., Lécuyer, C., Sucheras-Marx, B., Duarte,
745 L.V., Philippe, M., Reggiani, L., Martineau, F., 2010. Secular
746 environmental precursors to Early Toarcian (Jurassic) extreme
747 climate changes. Earth Planet. Sci. Lett. 290 (3–4), 448–458.
748 Svensen, H., Planke, S., Chevallier, L., Malthe-Sørenssen, A., Corfu, F.,
749 Jamtveit, B., 2007. Hydrothermal venting of greenhouse gases
750 triggering Early Jurassic global warming. Earth Planet. Sci. Lett. 256
751 (3–4), 554–566.
752 Sweere, T., van den Boorn, S., Dickson, A.J., Reichart, G.J., 2016.
753 Definition of new trace-metal proxies for the controls on organic
754 matter enrichment in marine sediments based on Mn, Co, Mo and Cd

755 concentrations. Chemical Geology 441, 235–245.
756 Tanabe, K., 1991. Early Jurassic macrofauna of the oxygen-depleted
757 epicontinental marine basin in the Toyora area, west Japan. Saito Ho-
758 On Kai Special Publication 3, 147–161.
759 Them II, T.R., Gill, B.C., Caruthers, A.H., Gerhardt, A.M., Gröcke, D.R.,
760 Lyons, T.W., Marroquín, S.M., Nielsen, S.G., Trabucho Alexandre,
761 J.P., Owens, J.D., 2018. Thallium isotopes reveal protracted anoxia
762 during the Toarcian (Early Jurassic) associated with volcanism,
763 carbon burial, and mass extinction. Proc. Natl. Acad. Sci. USA 115
764 (26), 6596–6601.
765 Toth, D.J., Lerman, A., 1977. Organic matter reactivity and sedimentation
766 rates in the ocean. Am. J. Sci. 277 (4), 465–485.
767 van de Schootbrugge, B., McArthur, J.M., Bailey, T.R., Rosenthal, Y.,
768 Wright, J.D., Miller, K.G., 2005. Toarcian oceanic anoxic event: An
769 assessment of global causes using belemnite C isotope records.
770 Paleoceanography 20, PA3008.
771 Westrich, J.T., Berner, R.A., 1988. The effect of temperature on rates of
772 sulfate reduction in marine sediments. Geomicrobiology Journal 6,
773 99–117.
774 Wignall, P.B., Newton, R.J., Little, C.T., 2005. The timing of
775 paleoenvironmental change and cause-and-effect relationships during
776 the Early Jurassic mass extinction in Europe. Am. J. Sci. 305 (10),

1014–1032.

Wignall, P.B., Bond, D.P., Kuwahara, K., Kakuwa, Y., Newton, R.J., Poulton, S.W., 2010. An 80 million year oceanic redox history from Permian to Jurassic pelagic sediments of the Mino-Tamba terrane, SW Japan, and the origin of four mass extinctions. Glob. Planet. Chang. 71, 109–123.

Wijsman, J.W.M., Middelburg, J.J., Heip, C.H.R., 2001a. Reactive iron in Black Sea sediments: implications for iron cycling. Marine Geology 172, 167–180.

Wijsman, J.W.M., Middelburg, J.J., Herman, P.M.J., Böttcher, M.E., Heip, C.H.R., 2001b. Sulfur and iron speciation in surface sediments along the northwestern margin of the Black Sea. Marine Chemistry 74, 261–278.

Woodfine, R.G., Jenkyns, H.C., Sarti,M., Baroncini, F., Violante, C., 2008. The response of two Tethyan carbonate platforms to the early Toarcian (Jurassic) oceanic anoxic event: environmental change and differential subsidence. Sedimentology 55, 1011–1028.

Wu, N., Farquhar, J., Strauss, H., Kim, S.T., Canfield, D.E., 2010. Evaluating the S-isotope fractionation associated with Phanerozoic pyrite burial. Geochimica et Cosmochimica Acta 74, 2053–2071.

Figures

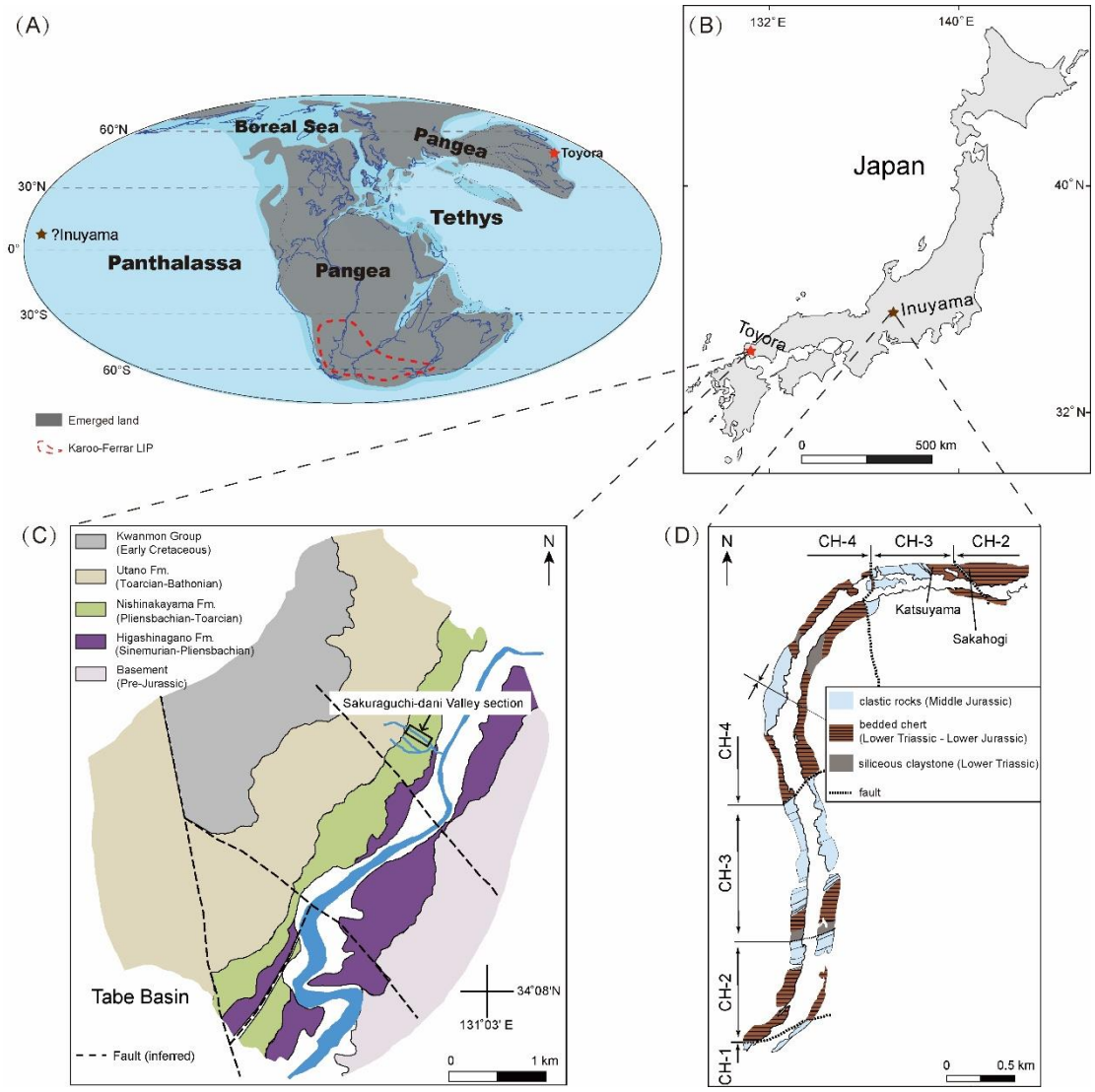

Fig. 1. (A). Paleogeographic map showing the locations of the Toyora (red star, Sakuraguchi-dani section) and Inuyama (brown star, Sakahogi section) sites in the Jurassic. Modified from Golonka (2007) and Scotese (2001). (B). Map of Japan showing the modern locations of the Toyora (red star) and Inuyama (brown star) field areas. (C). Geological map showing the Sakuraguchi-dani section in the Tabe Basin, Toyora area. Redrawn from Kemp and Izumi (2014). (D). Geologic map showing the Sakahogi

809 section and Katsuyama section of the Inuyama area. Redrawn from Ikeda

810 et al. (2018).

811

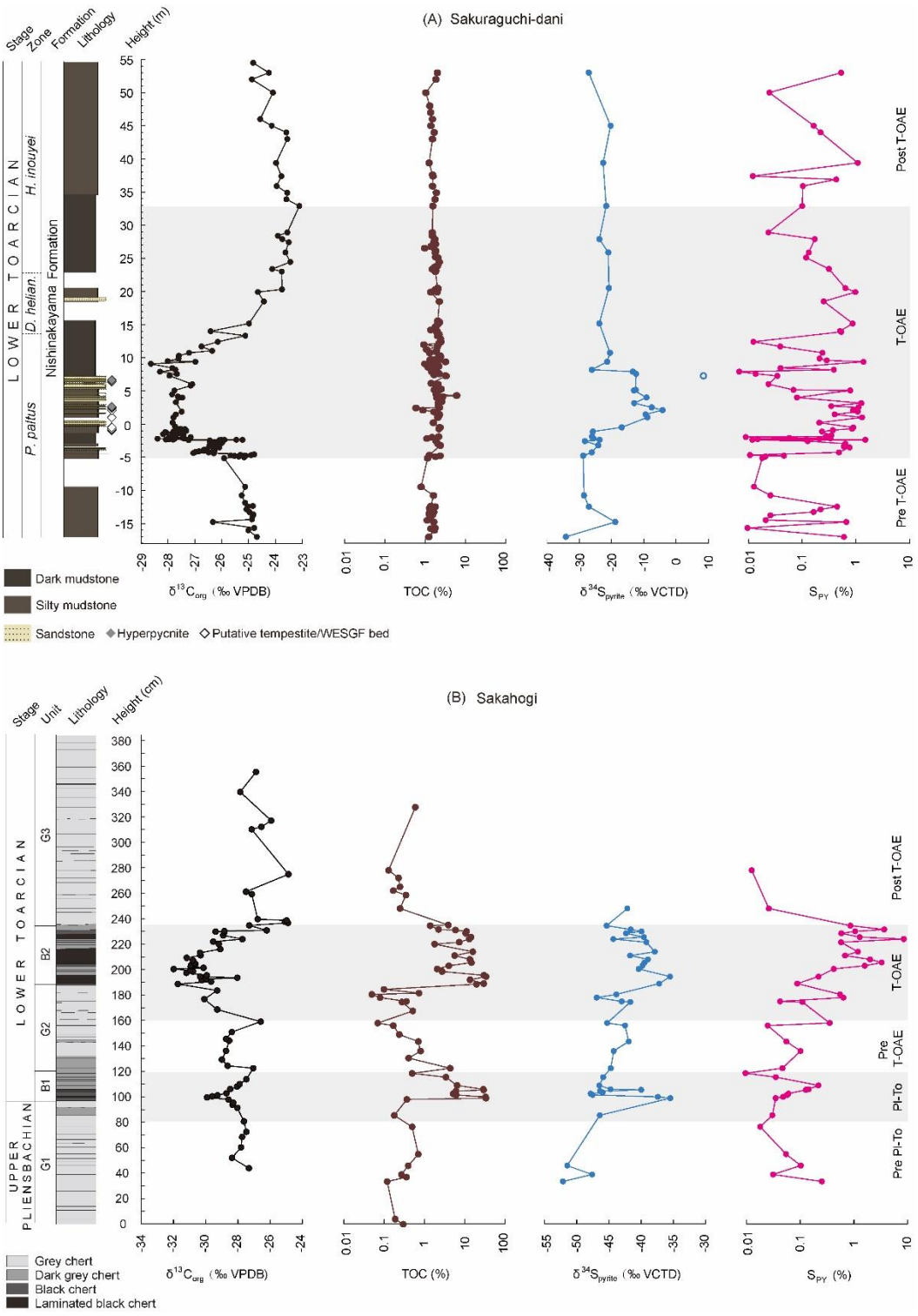

Fig. 2. Integrated organic carbon isotope ($\delta^{13}C_{org}$), total organic carbon (TOC), pyrite sulfur isotope ($\delta^{34}S_{pyrite}$), and pyrite sulfur (S_{py}) concentrations chemostratigraphy of the upper Pliensbachian-lower Toarcian at Sakuraguchi-dani (A) and Sakahogi (B), Japan. $\delta^{13}C_{org}$, TOC,

and lithostratigraphy at Sakuraguchi-dani are from Kemp and Izumi (2014) and Izumi et al. (2012, 2018a). Biostratigraphy is based on Nakada and Matsuoka (2011). $\delta^{13}C_{org}$, stratigraphic units, and lithostratigraphy at Sakahogi are from Ikeda et al. (2018) and references therein. TOC data at Sakahogi are from Kemp et al. (2022). Note that the unfilled blue circle in the Sakuraguchi-dani pyrite sulfur isotope profile represents the outlying value, and that the TOC and S_{PY} values in both sections are shown on logarithmic scales.

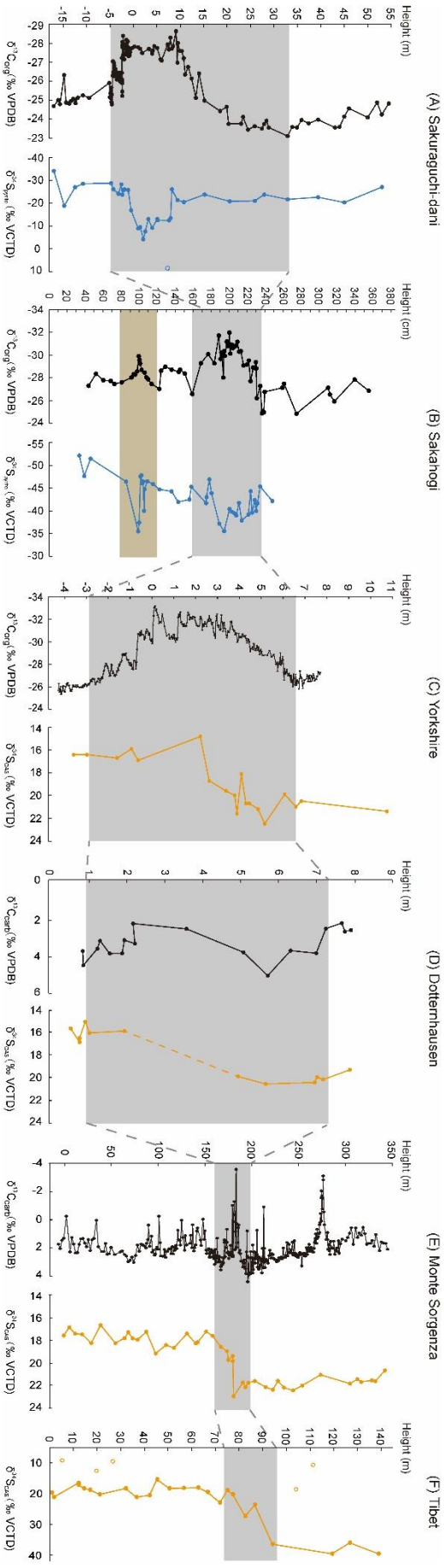
(A) Sakuraguchi-dani
(B) Sakahogi
(C) Yorkshire
(D) Dotternhausen
(E) Monte Sorgenza
(F) Tibet
Height (m)
Height (cm)
δ13Corg (‰ VPDB)
δ34Spyr (‰ VCTD)
δ34Scas (‰ VCTD)
δ13Ccarb (‰ VPDB)

827 Fig. 3. Excursions of $\delta^{13}C_{org}$, $\delta^{13}C_{carb}$, $\delta^{34}S_{pyrite}$, and $\delta^{34}S_{CAS}$ across the T-
828 OAE (dark grey areas) from Sakuraguchi-dani (A), Sakahogi (B),
829 Yorkshire (C), Dotternhausen (D), Monte Sorgenza (E) and Tibet (F). Note
830 that $\delta^{34}S_{pyrite}$ data are shown as blue solid circles (the blue hollow circle at
831 Sakuraguchi-dani represents an outlying value) and $\delta^{34}S_{CAS}$ data are shown
832 as orange solid circles (the orange hollow circles at Tibet represent outlying
833 values). The brown area at Sakahogi (B) denotes the Pl-To boundary.
834 $\delta^{13}C_{org}$ data at Yorkshire are from Cohen et al. (2004) and Kemp et al.
835 (2005). $\delta^{34}S_{CAS}$ data at Yorkshire are from Newton et al. (2011). $\delta^{13}C_{carb}$
836 and $\delta^{34}S_{CAS}$ data at Dotternhausen are from van de Schootbrugge et al.
837 (2005) and Gill et al. (2011), respectively. $\delta^{13}C_{carb}$ and $\delta^{34}S_{CAS}$ data at
838 Monte Sorgenza are from Woodfine et al. (2008) and Gill et al. (2011),
839 respectively. $\delta^{34}S_{CAS}$ data at Tibet are from Newton et al. (2011).
840

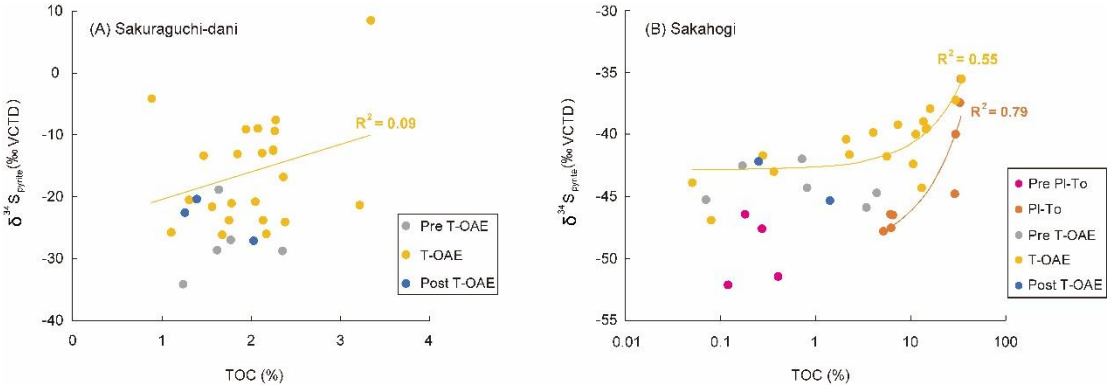

841

842 Fig. 4. Cross-plots of TOC and $\delta^{34}S_{pyrite}$ from the Sakuraguchi-dani section
843 (A) and the Sakahogi section (B). The R^2 in each plot is the linear
844 coefficient of determination. Note that TOC data from the Sakahogi section
845 are shown on a logarithmic scale.

846